Analyst

PAPER

View Article Online
View Journal

Cite this: DOI: 10.1039/d5an01268f

Molecular imprinting of aptamer/carbamazepine complexes for the development of an optical nanosensor

Iqra Salim, Eleanor Fiona Richards and Jon Ashley *

Monitoring anti-seizure medications (ASMs) such as carbamazepine is important to ensure that the correct dosage is given to patients, which provides the maximum therapeutic effect. However, therapeutic windows for carbamazepine are narrow and need to be highly tailored towards the patients. Therefore, there is a need for more precise analytical methods for monitoring ASMs. Here we report a new hybrid aptamer/molecularly imprinted nanoparticle (nanoMIP) optical nanosensor utilising fluorescence quenching for the detection of carbamazepine. The nanosensor relies on a co-operative based binding mechanism whereby when the aptamer binds to carbamazepine, it undergoes structural switching to change its 3D conformation and binds to the nanoMIP. Using a solid-phase imprinting technique, we synthesized nanoMIPs that recognise and bind to the aptamer/carbamazepine complexes. The resultant nanoMIPs can then selectively recognise and bind to the aptamer complex, resulting in a switch-off signal. The sensor demonstrated a limit of detection (LOD) of 12.7 nM and excellent sample recoveries of around 95% in 50% human serum.

Received 1st December 2025,
Accepted 27th February 2026

DOI: 10.1039/d5an01268f

rsc.li/analyst

Introduction

Carbamazepine is a first-line anti-seizure medication (ASM) widely prescribed for epilepsy, trigeminal neuralgia, and bipolar disorder. Carbamazepine is classified as a narrow spectrum ASM and is used to treat focal or partial seizures.[1] In healthcare, reliable carbamazepine measurement underpins therapeutic drug monitoring to mitigate dose-related toxicity, determine the maximum therapeutic effect and ensure seizure control.[2]

These clinical imperatives make sensitive, selective, and rapid determination of carbamazepine an ongoing analytical priority.

Conventional carbamazepine assays such as liquid chromatography mass spectrometry (LC-MS) offer excellent sensitivity and selectivity but at the cost of sophisticated instrumentation, trained personnel, lengthy sample preparation, and limited portability.[2–6] Other separation methods reported for the quantification of carbamazepine include high-performance liquid chromatography (HPLC)[7] and capillary electrophoresis.[8] The use of immunoassays and enzyme-linked formats for carbamazepine detection and quantification reduces time-to-result yet can suffer from antibody cross-reactivity, batch-to-batch variability, and cold-chain constraints.[9,10] Biosensors such as electrochemical[11] and optical sensors[12] have emerged as attractive alternatives for therapeutic drug monitoring; however, many reported platforms still face challenges, including sluggish electron-transfer kinetics, surface fouling in complex media, and insufficient discrimination against structurally related interferents such as carbamazepine-10,11-epoxide, oxcarbazepine, and common co-medications.[13] Other notable biosensor platforms for the detection of carbamazepine include fluorescence polarisation[14] and the use of copper-based nanocomposites.[15]

Aptamers and molecularly imprinted polymers have emerged as exciting chemical antibodies due to their flexibility in terms of functionality and stability as biorecognition elements in biosensors.[16] Several studies have focused on the development of biosensors for the detection of anti-seizure medications utilising these chemical antibodies as effective biorecognition elements. In 2022, Chung *et al.* developed an electrochemical aptasensor for the detection of carbamazepine, achieving detection limits of 1.25 and 1.82 nM for 5 and 30 min assays, respectively.[17] In terms of MIPs, researchers developed molecularly imprinted polymers on carbon paste electrodes to monitor phenobarbital, carbamazepine, and levetiracetam.[18]

Attempts to combine aptamers and MIPs have resulted in the formation of hybrid aptaMIPs in the field of nanosensors,

School of Pharmaceutical and Biomolecular Sciences, Liverpool John Moores University, 3 Byrom Way, Liverpool, L3 3AF, UK. E-mail: j.ashley@ljmu.ac.uk

which allows for the synergistic effects of both aptamers and MIPs, enhancing performance as a multifunctional nanomaterial.[19] These hybrid aptaMIPs have been demonstrated as biorecognition elements in biosensors and as sorbent materials in a number of sensor applications.[20–22]

Hybrid aptaMIP materials have been developed for a variety of target analytes such as viruses, proteins and small molecules.[23,24] In 2022, researchers developed a label-free electrochemical nanohybrid MIP aptasensor utilising molecular organic frameworks to detect the Covid-19 virus.[25] The nanosensor demonstrated a LOD of 3.3 ± 0.04 PFU mL^{-1} in electrochemical detection.

In 2016, Jolly *et al.* utilised an electrochemical sensor for the detection of prostate specific antigens.[26] Using a thiolated aptamer and synthesising the MIP through the electro-polymerisation of dopamine, the researchers fabricated a film-based hybrid material that was able to detect prostate specific antigen (PSA) down to a LOD of 1 pg mL^{-1} (0.029 pM). More recently, Turk *et al*. demonstrated the electrochemical detection of thrombin using multiwalled carbon nanotubes as the substrate for a MIP/aptamer hybrid.[27] The multifunctional material was capable of detecting thrombin down to 1.4 pg mL^{-1} (0.038 pM).

To date, strategies for creating hybrid nanoMIP/aptamer materials have included utilising chemically modified aptamers with polymerizable groups and terminally functionalised aptamers. The most common method has been to modify the terminal group of the aptamers with a polymerizable moiety and treat the aptamer as a functional macromonomer.[22]

Hybrid aptamer molecularly imprinted polymer nanoparticles were also developed against oxidized low-density lipoproteins as a strategy for reducing internalisation by macrophages.[28]

Another approach was demonstrated by Sullivan *et al.* who took the antibiotic moxifloxacin and chemically modified thymine groups throughout the aptamer to convert the aptamer into a multi-sited crosslinker which was then incorporated into the MIP using solid phase imprinting.[29] Another approach used specifically for electrochemical sensors is to use terminally functionalised aptamers and bioconjugate the aptamer to a gold electrode surface.[26,30] The aptamer functionalised gold electrode is then electropolymerized using thionine or dopamine as monomers.

Recently, we demonstrated a strategy for the synthesis of hybrid aptaMIP materials (also known as nanoMIP beacons) where the aptamer is incorporated as part of the template rather than as a functional monomer.[31] This approach allows for a unique bio-recognition through a pseudo co-operative binding mechanism where the aptamer is used as a ligand that first recognises the analyte. Upon binding the analyte, the 3D conformation of the aptamer in its complex changes (structure-switching[32]), which can then be recognised by the MIP. This strategy provides a convenient way to incorporate aptamers and MIPs into sandwich-based assays whereby the MIP mimics the capture antibody and the aptamer acts as the reporter.

Here, we report an optical based nanosensor for the detection of carbamazepine that integrates an aptamer containing a black hole quencher and 5′ labelled amino groups and MIP integrated with a fluorescent-labelled monomer. When the aptamer binds to the carbamazepine causing its 3D conformation to change through structure-switching, the aptamer–carbamazepine complex is recognised by the nanoMIP and binds, causing a switch-off signal. In contrast, the aptamer in its unbound state showed little binding towards the nanoMIP, demonstrating a co-operative based binding mechanism and improved selectivity and robustness compared to aptamer-and MIP-only biosensors. The developed nanosensor will act as the basis for point-of-care (POC) monitoring of ASMs in clinically relevant samples.

Experimental

Materials and methods

The carbamazepine-binding aptamer sequence was adapted from a previously published, structurally switching design.[17] Both the target aptamer and a scrambled sequence (SS) oligonucleotide were obtained from Integrated DNA Technologies (IDT) with the following sequences. The carbamazepine aptamer sequence corresponds to /5AmMC6/5′-CGA GGC TCT CGG GAC GAC GGG GCA CGG GCC TCT GGG TCG GCA TGG CCC GTC GTC CCG CCT TTA GGA TTT ACA G 3′ /3BHQ_1/ while the SS corresponds to /5AmMC6/CTA CGC GCG CAG CTG TCG AGG TAT CTT CCT ATT GGC CGC GTG TCG CCG ACC CGA ATG GCG AGC GGT GGC GGC /3BHQ_1/. Here, /5AmMC6/ denotes a 5′ amino modifier and /3BHQ_1/ is a 3′ black hole quencher 1. For solid support functionalisation, soda lime glass beads (Potters; Spheriglass A glass 2429 CP 00) were sourced from Silmid (UK). 3-Glycidyloxypropyltrimethoxysilane (GPTMS) and toluene were purchased from Sigma Aldrich.

NanoMIP synthesis employed the following monomers and cross linkers: *N*-isopropylacrylamide (NIPAm), *N*-*tert*-butylacrylamide (TBAm), acrylic acid (AAc), *N*-(3 aminopropyl) methacrylamide HCl (APM), and *N*,*N*′-methylenebisacrylamide (BIS). Polymerisation was initiated with ammonium persulfate (APS) and catalysed with *N*,*N*,*N*′,*N*′-tetramethylethylenediamine (TEMED). Fluorescein O-acrylate was included for fluorescent labelling and all monomers and crosslinkers were obtained from Sigma Aldrich. Carbamazepine, diclofenac, ethosuximide and sodium valproate were purchased from Sigma Aldrich. Carbamazepine 10,11-epoxide (carbamazepine epoxide) was purchased from BioSynth UK. Sample recovery experiments were performed using human serum from Sigma Aldrich. Fluorescence measurements were carried out on a Tecan Synergy plate reader or CLARIOstar Plus using black 96 well plates, with excitation at 465 nm and emission collected from 500 to 610 nm (gain 80, bandwidth 20 nm). Transmission electron microscopy (TEM) images were acquired on a Field Electron and Ion Company (FEI) Morgagni instrument.

Functionalisation of glass beads with carbamazepine aptamers

Glass beads (70 g) were pre-cleaned with 1 M NaOH, rinsed with water to neutrality, and dried. Beads were then silanised by incubation with 2% (v/v) GPTMS in anhydrous toluene for 48 h. The resulting epoxide-terminated beads were washed with 8 × 30 mL portions of acetone and dried under vacuum. To immobilise the capture probe, beads were incubated overnight with 20 μM amine terminated carbamazepine aptamer in carbonate buffer (pH 9.0). Residual epoxide groups were capped using 1 mM ethanolamine. Beads were finally washed with eight 30 mL portions of water and stored in 50 mM Tris buffer (pH 7.4) at 4 °C.

Synthesis of nanoMIPs for carbamazepine

Fluorescent nanoMIPs targeting carbamazepine aptamer complexes were produced using a modified, chemically initiated solid-phase imprinting approach.[33] Aptamer functionalised glass beads (70 g) were incubated with 10 mM carbamazepine in 50 mM Tris buffer (pH 7.4) for 1 h to form the aptamer–ligand complexes on the glass beads. The supernatant was removed under vacuum and the decrease in absorbance (pre *vs*. post incubation) was recorded by UV spectrometry to verify complex formation.

A 100 mL pre-polymerisation solution containing NIPAm (0.34 mmol), AAc (0.032 mmol), TBAm (0.26 mmol), BIS (0.013 mmol), APM (0.06 mmol), fluorescein-O-acrylate (1.29 μmol), and 10 μM carbamazepine in 50 mM Tris buffer (pH 7.4) was prepared and degassed by nitrogen for 30–60 min. Separately, the bead bed was degassed by vacuum sonication for 30 min. 30 mL of the pre-polymerisation mixture was then percolated through the bead bed. Polymerisation was initiated by first adding TEMED (30 μL), followed by 500 μL of APS solution (10%). The reaction proceeded for 16 h with overhead stirring using a paddle designed to sit within the solid-phase cartridge in the liquid overlayer.

Beads were rinsed with eight bed volumes of deionised water to remove unreacted species, low affinity material, and free carbamazepine imprinted nanoparticles. High affinity nanoMIP beacons were subsequently eluted by incubating the bead column in pre-warmed water (60 °C) for 15 min and collecting the eluate under vacuum. This elution was performed three times. Final nanoMIP preparations were stored at 4 °C until use.

Glass beads for the synthesis of a positive nanoMIP control were prepared in the same manner but without carbamazepine during the aptamer incubation and in the pre-polymerisation mixture. The absence of residual (leached) carbamazepine was confirmed by ultraviolet (UV) absorption (Fig. S2). Glass beads were regenerated by soaking in water for 2–4 h followed by ten 30 mL washes with deionised water.

Characterisation of nanoMIP beacons

NanoMIPs were characterised using TEM by depositing 10 μL of sample onto Formvar coated TEM grids which were left to dry overnight. NanoMIPs were also characterised using fluorescence spectroscopy. NanoMIPs were scanned at different concentrations (0.01–0.25 mg mL^{-1}). The effect of aptamer concentration on the fluorescence quenching of the nanoMIP was determined by incubating the nanoMIP (50 μL, 0.25 mg mL^{-1}) with 50 μL of either the carbamazepine aptamer or SS at different concentrations (10–10 000 nM) in 50 mM tris buffer pH 7.4. The extent of binding and quenching was also determined for the positive nanoMIP control by incubating 50 μL of the positive nanoMIP control with 50 μL of the carbamazepine aptamer at different concentrations (10–10 000 nM) in 50 mM Tris buffer pH 7.4.

Fluorescence quenching assay

All fluorescence quenching assays were performed in triplicate. The response of the aptamer in the presence of the nanoMIP was assessed by mixing a fixed concentration (100, 1000 or 5000 nM) of the carbamazepine aptamer tagged with a quencher or SS tagged with a quencher, respectively, with 1 mL (0.25 mg mL^{-1}) of nanoMIP beacon in 50 mM Tris buffer pH 7.4. To each well, 50 μL of this solution was incubated with different concentrations of carbamazepine (45–1200 nM) and the fluorescence scans and fluorescence intensity were measured. The extent of fluorescence quenching was determined using the Stern–Volmer equation by plotting the ratio $[(I_0/I) - 1]$ against carbamazepine concentration (nM).

The selectivity of the sensor was determined by incubating a premix of carbamazepine aptamer or SS (5 μM) with 1 mL of nanoMIP beacon (0.25 mg mL^{-1}) in 50 mM tris buffer pH 7.4. 50 μL of this solution was incubated with the highest concentration of each ASM (15 μM) and the extent of fluorescence quenching was measured from the $[(I_0/I) - 1]$ ratio *vs*. the concentration of carbamazepine.

The ability of the nanoMIP beacons to detect carbamazepine in 50% diluted human serum samples was assessed by determining the sample recoveries of carbamazepine in the presence of the aptamer ligand and nanoMIP beacon. Sample recoveries were determined by premixing 5 μM of carbamazepine aptamer or SS with 1 mL of nanoMIP (0.25 mg mL^{-1}) in 50 mM Tris buffer pH 7.4. 50 μL of this solution was incubated with spiked concentrations of carbamazepine (100, 500 and 1200 nM) in 50% human serum and compared to the unspiked sample. The stability of nanoMIP fluorescence was assessed by measuring the fluorescence of 100 μL of nanoMIP beacon (0.25 mg mL^{-1}) at 0, 1, 2, 4, 8, 12, and 24 h. The normalized fluorescence change was calculated as $\Delta F/F_0 = (F_t - F_0)/F_0$, where F_0 is the mean fluorescence at 0 h and F_t is the mean fluorescence at each subsequent timepoint. Fluorescence measurements were obtained, and the fluorescence quenching was determined from the Stern–Volmer ratio $[(I_0/I) - 1]$. The found concentrations were determined by extrapolation of the Stern–Volmer ratio from the linear Stern–Volmer plot, and the unspiked sample was assumed to be zero.

Results and discussion

In this work, we developed nanoMIPs against carbamazepine/carbamazepine complexes. The mechanism of transduction occurs when the aptamer recognises and binds the carbamazepine analyte, resulting in a change in the 3D structure of the aptamer. The aptamer in its bound state is recognised and binds to the nanoMIP, causing the black hole quencher on the aptamer to come into close proximity to the fluorescent nanoMIP, resulting in the quenching of the nanoMIP fluorescent signal.

Functionalisation of glass beads

We utilized a previously described technique called solid-phase imprinting in order to synthesize aptamer/carbamazepine nanoMIPs (Scheme 1).

The solid-phase imprinting technique allows for the aptamer adopt a single orientation *via* nucleophilic conjugation of the amino-terminated aptamer to epoxide-bearing glass beads. When thiolated aptamers were initially used, reduction of the disulphide groups with (tris(2-carboxyethyl) phosphine) (TCEP) gave rise to an undesirable side reaction on the black hole quencher with loss of colour, suggesting that thiolated aptamers are incompatible with black hole quenchers as dual terminal functional groups on the aptamer. Therefore, aptamers with an amino group on the 5′ end and a black hole quencher on the 3′ end were immobilised onto the epoxide functionalised glass beads. To effectively immobilise these aptamers, a high pH carbonate buffer at pH 9.0 was used. The functionalisation of the carbamazepine aptamers on the glass beads was confirmed after incubation by comparing the intensity of the aptamer band on a native PAGE gel (Fig. 1S). Nanodrop optical density (OD) measurements were also performed at 260 nm to confirm the functionalisation of the aptamer on the glass beads. Carbamazepine was incubated with the glass beads in order to form the aptamer/carbamazepine template. The formation of the aptamer/carbamazepine template on the glass beads was confirmed using a UV spectrometer before and after incubation (Fig. S2) and subsequent washes. Glass beads containing the aptamer on its own were also prepared for the synthesis of the nanoMIP positive control (formed in the absence of carbamazepine). Pre-polymerisation mixtures were prepared containing functional monomers, a fluorescein labelled monomer, a crosslinker and a free carbamazepine template. The pre-polymerisation mixture was also buffered in Tris buffer at 7.4 pH to prevent hydrolysis of the DNA aptamer at low pH by acrylic acid. NanoMIPs were synthesized using chemical-based polymerisation with TEMED and APS with different concentrations of the fluorescent monomer.

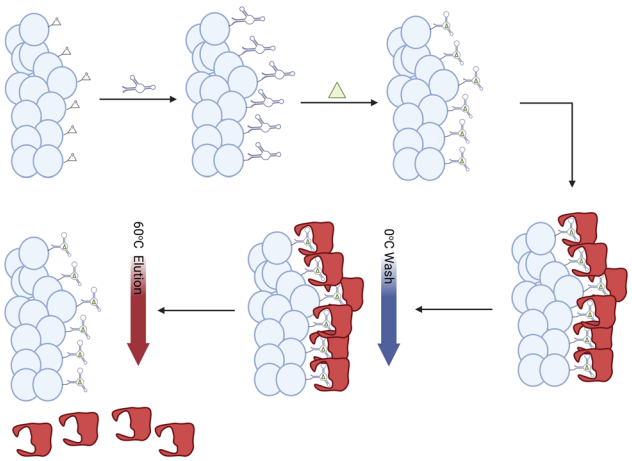

Scheme 1 Overview of the solid-phase synthesis technique for synthesizing nanoMIPs against carbamazepine aptamer complexes.

Characterisation of the fluorescent nanoMIPs

The synthesized nanoMIPs were characterised by TEM (Fig. 1A and B). Particles were found to have round morphologies and an average diameter of about 100 nm. The use of dynamic light scattering (DLS) was not possible due to the interference from the fluorophore in the measurements. Average yield from the chemical polymerisation was estimated to be 0.14 ± 0.01 mg g^{-1} glass beads from 3 replicate batches based on the average amount of freeze-dried nanoMIPs. The glass beads were regenerated and reused for at least 5 batches.

The co-operative binding mechanism and fluorescence properties of the nanoMIPs were recorded and optimised on the fluorescence plate reader. The fluorescence signal was recorded for the nanoMIPs in the presence of different concentrations of carbamazepine aptamers and scrambled sequences (SS) in the absence of carbamazepine respectively. The fluorescence scans for the nanoMIPs in the presence of both carbamazepine aptamers (Fig. 2A) and scrambled sequences (SS) (Fig. 2B) demonstrated only a small decrease in signal, which can be attributed to dynamic quenching, confirming that neither the aptamer or the SS control bind strongly to the nanoMIPs up to a maximum concentration of 10 μM, when carbamazepine analyte is absent. In contrast, the positive nanoMIP control (Fig. 2C), synthesized against the carbamazepine aptamer only, showed a significant quenching effect in fluorescence with increasing carbamazepine aptamer concentration in the absence of the carbamazepine analyte. When comparing the fluorescence of the nanoMIP and positive

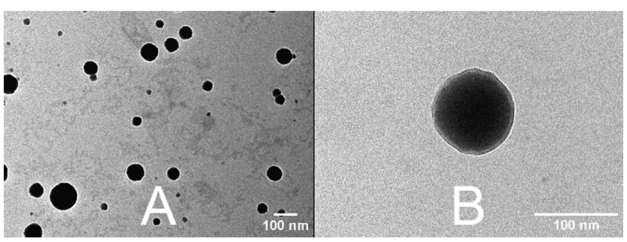

Fig. 1 Transmission electron microscopy (TEM) images of carbamazepine/aptamer-selective nanoMIPs (60–100 nm diameter from three independent batches): (A) representative field of view; (B) higher-magnification image.

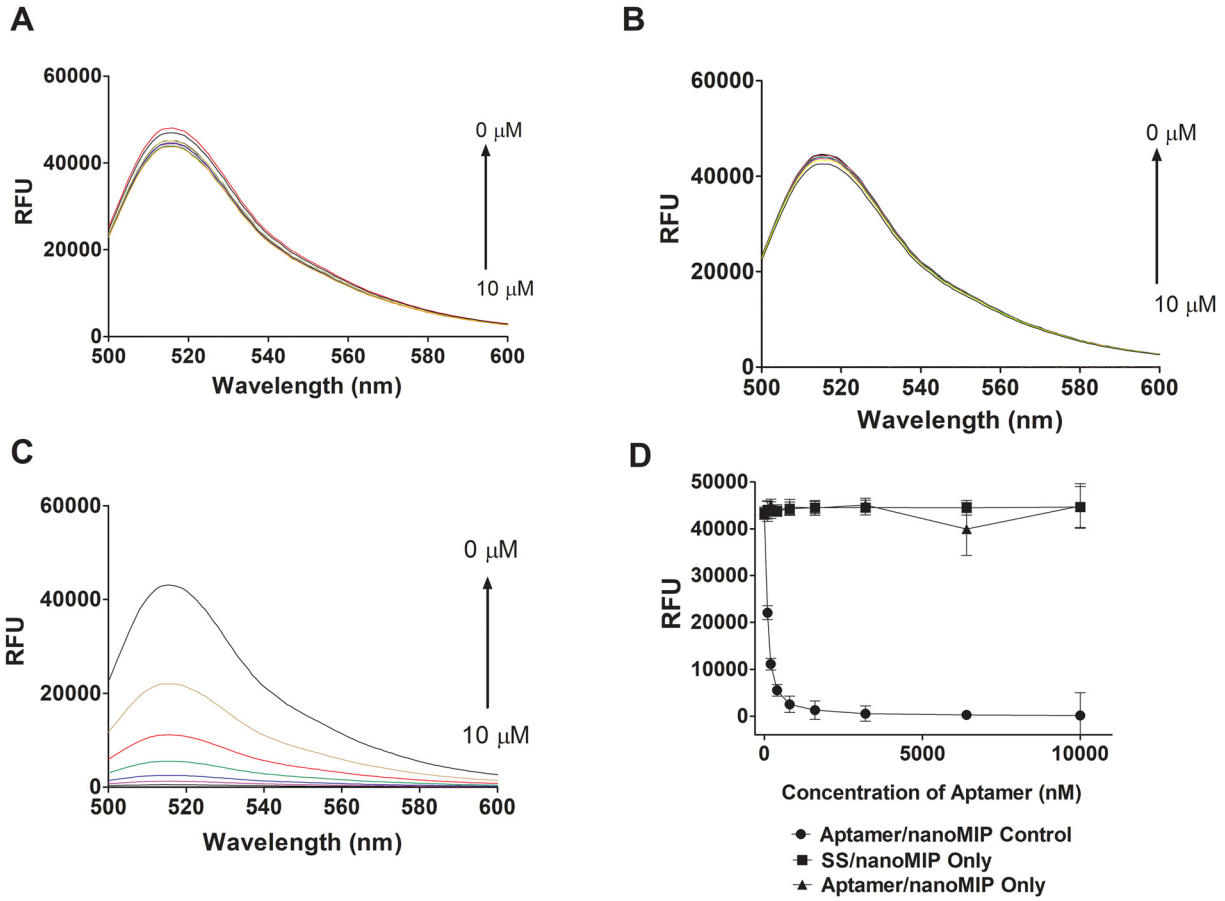

Fig. 2 Fluorescence quenching of nanoMIPs with increasing concentrations of (A) carbamazepine aptamer (no carbamazepine), (B) scrambled sequence (SS); (no target), (C) positive nanoMIP control with increasing carbamazepine aptamer concentration, and (D) fluorescence signal *versus* aptamer concentration (0–10 000 nM, n = 3).

nanoMIP control in the presence of either the aptamer or SS (Fig. 2D), we can confirm that the aptamer does not bind to the nanoMIP in its unbound state and there is little to no non-specific binding by the SS, and if carbamazepine is absent during the imprinting of the positive nanoMIP control, the carbamazepine aptamer can be recognised in its unbound conformation. As with most structure switching-based aptamers, carbamazepine undergoes a change in 3D conformation when it binds to the carbamazepine analyte, which is thermodynamically more favourable than the aptamer in its unbound state, which could only be partially folded or could exist in alternative folded conformations.

NanoMIP assay design

Next, we developed the nanoMIP assay by incubating the nanoMIPs with different concentrations of carbamazepine and a fixed concentration of aptamer (5 μM) or SS (5 μM) and measuring the changes in the fluorescence signal. Scans of the quenching effect of the nanoMIPs incubated with the carbamazepine aptamer and SS in the presence of increasing concentrations of carbamazepine are shown in Fig. 3A and B. As the concentration of carbamazepine was increased, the degree of fluorescence quenching increased when the aptamer was present with the nanoMIP in comparison with the SS control, which showed little to no fluorescence quenching (Fig. 3C). The corresponding Stern–Volmer plots (Fig. 3D) for the linear concentration range for both the carbamazepine aptamer and SS also demonstrated a high degree of quenching for the carbamazepine aptamer when compared to the SS control. The Stern–Volmer constant was found to be K_{Sv} = 2.276 × 10^{-4} nM^{-1} for the developed nanoMIP beacons in the presence of the carbamazepine aptamer plotted against the carbamazepine concentration.

The dynamic range of the nanoMIPs was determined to be between 45 and 1200 nM and the limit of detection (LOD) was determined from the standard deviation of 3 blank samples. The LOD was determined to be 12.7 ± 2.6 nM under optimal buffer conditions.

The selectivity of the nanoMIPs were determined by incubating a fixed concentration of aptamer (5 μM) with each ASM (15 μM) and measuring the degree of quenching of the nanoMIPs, as shown in Fig. 4.

The nanoMIPs showed a significant amount of quenching with carbamazepine in the presence of the aptamer and little

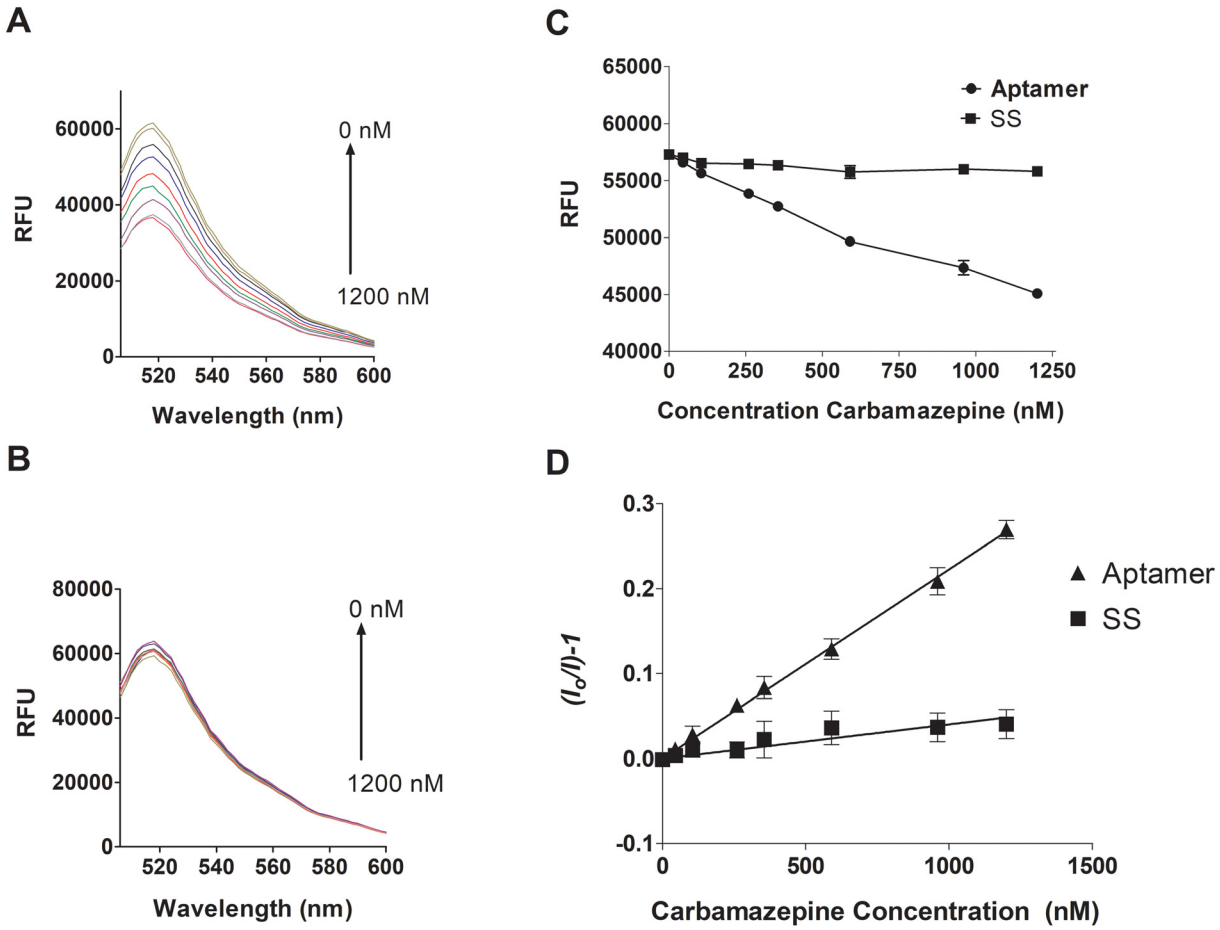

Fig. 3 Carbamazepine quantification by fluorescence quenching of nanoMIPs in the presence of 5 μM carbamazepine aptamer or scrambled sequence (SS) and increasing carbamazepine (45–1200 nM), (n = 3). (A) Emission spectra of nanoMIPs with 5 μM carbamazepine aptamer and carbamazepine (45–1200 nM); (B) emission spectra of nanoMIPs with 5 μM SS and carbamazepine (45–1200 nM); (C) fluorescence signal change of nanoMIPs with 5 μM SS across the carbamazepine range (45–1200 nM) and (D) Stern–Volmer plots for nanoMIP quenching as a function of carbamazepine concentration in the presence of the carbamazepine aptamer (r^2 = 0.9853) and SS (r^2 = 0.93442), where $((I_0/I) - 1) = K_{SV}[Q]$.

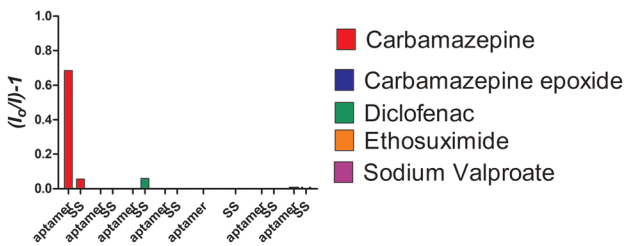

Fig. 4 Selectivity of nanoMIPs towards different ASMs in the presence of both the SS and carbamazepine aptamer, respectively (n = 3).

to zero signal change when the nanoMIPs were incubated with other ASMs. The lack of fluorescence quenching was most striking in the case of carbamazepine epoxide which has a similar structure to carbamazepine. There was also very little quenching of the nanoMIP signal in the presence of the SS and all ASMs.

Finally, we assessed the accuracy of the sensor in simulated human serum samples by spiking different concentrations of carbamazepine into 50% human serum to represent concentrations across the linear range within the linear dynamic range (100, 500, and 1000 nM) and a fixed concentration of aptamer (5 μM). Table 1 shows that the sample recoveries were measured and varied between 95.6 and 96.1%. The precision of the sensor varied with an RSD of between 2.9 and 3.2%. These results suggest that the developed nanosensor is robust enough to be used in a clinical setting. The blank nanoMIP fluorescence signal was stable over 24 h, showing ~1.0% mean drift ($\Delta F/F_0$ = −0.99% from 0 to 24 h) with ~1% variability (pooled %CV ≈ 1.0%) (Fig. S3).

Table 1 Percentage recoveries of carbamazepine spiked into 50% human serum and the corresponding RSD values (n = 3)

Spiked concentration in 50% human serum	Observed concentration	Recovery %	RSD %
100	96 ± 1.23 nM	95.6	3.2
500	480 ± 3.5 nM	96	3.1
1000	960 ± 7.2 nM	96.1	2.9

Conclusion

In this article, we demonstrated the first imprinting of aptamer/carbamazepine complexes. The synthesized nanoMIPs were 60–100 nm in diameter and demonstrated a unique co-operative binding mechanism. The co-operative binding mechanism relies on the fact that the aptamer displays structure-switching capability in that the aptamer changes its 3D structure upon binding to carbamazepine. The nanoMIP is designed to recognise the aptamer/carbamazepine complex over the aptamer in its unbound state. The nanoMIP sensor showed low nanomolar detection limits and excellent selectivity towards carbamazepine compared to other ASMs including the structurally similar carbamazepine epoxide. The nanoMIP sensor also showed excellent recoveries in 50% human serum. Overall, this nanosensor could provide a viable route towards a synthetic ELISA owing to the fact that the aptamer can act as a reporter ligand while the nanoMIP nanosensor acts as a capture ligand. We are currently looking at converting this sensor into other types of platforms including electrochemical sensors. With larger templates such as whole proteins, the requirement for structure switching would not be needed due to the size difference between the protein and aptamer/protein complexes.

Author contributions

Iqra Salim: methodology and editing of the manuscript; Eleanor Fiona Richards: methodology; and Jon Ashley: conceptualisation, methodology, writing and editing of the manuscript, and supervision.

Conflicts of interest

There are no conflicts to declare.

Data availability

The data supporting this article have been included as part of the supplementary information (SI) and include fluorescence stability, UV absorption of carbamazepine and gel images of the aptamer. Supplementary information is available. See DOI: https://doi.org/10.1039/d5an01268f.

Data for this article, including fluorescence measurements and TEM images, are available at the LJMU data repository at https://opendata.ljmu.ac.uk/.

Acknowledgements

The authors would like to acknowledge the support of a CAMS Fellowship [grant number: 600310/22/06] from the Analytical Chemistry Trust Fund and the Community for Analytical Measurement Science for funding this work.

References

1 J. Martinho, A. Y. Simão, M. Barroso, E. Gallardo and T. Rosado, *Molecules*, 2024, **29**, 4679, DOI: 10.3390/molecules29194679.
2 D. Ma, Z. Ji, H. Cao, J. Huang, L. Zeng and L. Yin, *Molecules*, 2022, **27**, 1224, DOI: 10.3390/molecules27041224.
3 M. Hemida, A. Ghiasvand, V. Gupta, L. J. Coates, A. A. Gooley, H. J. Wirth, P. R. Haddad and B. Paull, *Anal. Chem.*, 2021, **93**, 12032–12040, DOI: 10.1021/acs.analchem.1c02193.
4 X.-S. Miao and C. D. Metcalfe, *Anal. Chem.*, 2003, **75**, 3731–3738, DOI: 10.1021/ac030082k#Abstract.
5 J. Taibon, R. Schmid, S. Lucha, S. Pongratz, K. Tarasov, C. Seger, C. Timm, R. Thiele, J. M. Herlan and U. Kobold, *Clin. Chim. Acta*, 2017, **472**, 35–40, DOI: 10.1016/j.cca.2017.07.013.
6 M. Koziarska, M. Strzebońska and E. Szalińska, *Sci. Rep.*, 2025, **15**, 1–17, DOI: 10.1038/s41598-025-15614-4.
7 R. G. Kelmann, G. Kuminek, H. F. Teixeira and L. S. Koester, *Chromatographia*, 2007, **66**, 427–430, DOI: 10.1365/s10337-007-0314-7.
8 Y. Y. Lin, C. C. Wang, Y. H. Ho, C. S. Chen and S. M. Wu, *Anal. Bioanal. Chem.*, 2013, **405**, 259–266, DOI: 10.1007/s00216-012-6481-x.
9 Y. Luo, M. Pehrsson, L. Langholm, M. Karsdal, A. C. Bay-Jensen and S. Sun, *Diagnostics*, 2023, **13**, 1835, DOI: 10.3390/diagnostics13111835.
10 V. Calisto, A. Bahlmann, R. J. Schneider and V. I. Esteves, *Chemosphere*, 2011, **84**, 1708–1715, DOI: 10.1016/j.chemosphere.2011.04.072.
11 V. Poza-Nogueiras, A. Puga, J. G. Pacheco and C. Delerue-Matos, *Talanta*, 2026, **299**, 129128, DOI: 10.1016/j.talanta.2025.129128.
12 N. Chen, Y. Yuan, P. Lu, L. Wang, X. Zhang, H. Chen and P. Ma, *Biomed. Opt. Express*, 2021, **12**, 7673–7688, DOI: 10.1364/BOE.440939.
13 E. Perucca, *Br. J. Clin. Pharmacol.*, 2006, **61**(13), 246–255, DOI: 10.1111/j.1365-2125.2005.02529.x.
14 L. Oberleitner, U. Dahmen-Levison, L. A. Garbe and R. J. Schneider, *J. Environ. Manage.*, 2017, **193**, 92–97, DOI: 10.1016/j.jenvman.2017.01.063.
15 F. Goudarzy, J. Zolgharnein and J. B. Ghasemi, *Inorg. Chem. Commun.*, 2022, **141**, 109512, DOI: 10.1016/j.inoche.2022.109512.
16 M. Naseri, M. Mohammadniaei, Y. Sun and J. Ashley, *Chemosensors*, 2020, **8**, 32, DOI: 10.3390/chemosensors8020032.
17 S. Chung, N. K. Singh, V. K. Gribkoff and D. A. Hall, *ACS Omega*, 2022, **7**, 39097–39106, DOI: 10.1021/acsomega.2c04865.
18 Aaryashree, A. Choudhary and Y. Yoshimi, *Sensors*, 2023, **23**(6), 3271, DOI: 10.3390/s23063271.
19 G. K. Ali and K. Omer, *Talanta*, 2022, **236**, 122878, DOI: 10.1016/j.talanta.2021.122878.

20 Z. Zhang and J. Liu, *Small*, 2019, **15**, 1–12, DOI: 10.1002/smll.201805246.
21 W. Bai, N. A. Gariano and D. A. Spivak, *J. Am. Chem. Soc.*, 2013, **135**, 6977–6984, DOI: 10.1021/ja400576p.
22 Z. Zhang and J. Liu, *ACS Appl. Mater. Interfaces*, 2016, **8**(10), 6371–6378, DOI: 10.1021/acsami.6b00461.
23 M. V. Sullivan, O. Clay, M. P. Moazami, J. K. Watts and N. W. Turner, *Macromol. Biosci.*, 2021, **21**, 2100002, DOI: 10.1002/mabi.202100002.
24 A. Poma, H. Brahmbhatt, H. M. Pendergraff, J. K. Watts and N. W. Turner, *Adv. Mater.*, 2015, **27**, 750–758, DOI: 10.1002/adma.201404235.
25 Z. Rahmati and M. Roushani, *Mikrochim. Acta*, 2022, **189**, 287, DOI: 10.1007/s00604-022-05357-8.
26 P. Jolly, V. Tamboli, R. L. Harniman, P. Estrela, C. J. Allender and J. L. Bowen, *Biosens. Bioelectron.*, 2016, **75**, 188–195, DOI: 10.1016/j.bios.2015.08.043.
27 F. Turk, A. Atilgan and N. Yildirim-Tirgil, *Anal. Lett.*, 2024, **57**, 383–396, DOI: 10.1080/00032719.2023.2209678.
28 S. Chunta, S. Khongwichit, P. Swangphon, M. Srisuk, P. A. Lieberzeit and M. Amatatongchai, *ACS Appl. Mater. Interfaces*, 2025, **17**(28), 40101, DOI: 10.1021/acsami.5c07018.
29 M. V. Sullivan, F. Allabush, D. Bunka, A. Tolley, P. M. Mendes, J. H. R. Tucker and N. W. Turner, *Polym. Chem.*, 2021, **12**, 4394–4405, DOI: 10.1039/d1py00607j.
30 S. Yang, Y. Teng, Q. Cao, C. Bai, Z. Fang and W. Xu, *J. Electrochem. Soc.*, 2019, **166**, B23–B28, DOI: 10.1149/2.0131902jes.
31 W. Goulding, Y. Sun and J. Ashley, *Biosens. Bioelectron.*, 2025, **267**, 116856, DOI: 10.1016/j.bios.2024.116856.
32 T. A. Feagin, N. Maganzini and H. T. Soh, *ACS Sens.*, 2018, **3**, 1611–1615, DOI: 10.1021/acssensors.8b00516.
33 F. Canfarotta, A. Poma, A. Guerreiro and S. Piletsky, *Nat. Protoc.*, 2016, **11**, 443–455, DOI: 10.1038/nprot.2016.030.